

Observations on K-image Expansion of Image-Mixing Augmentation for Classification

**Joonhyun Jeong^{*1}, Sungmin Cha^{*2}, Youngjoon Yoo^{1, 3},
Sangdoo Yun³, Taesup Moon², and Jongwon Choi⁴**

¹ Face, NAVER Colva, ² Seoul National University, ³ NAVER AI Lab, ⁴ Chung-Ang University
 {joonhyun.jeong, youngjoon.yoo, sangdoo.yun}@navercorp.com, {sungmin.cha, tsmoon}@snu.ac.kr, choijw@cau.ac.kr

Abstract

Image-mixing augmentations (e.g., Mixup or CutMix), which typically mix two images, have become de-facto training tricks for image classification. Despite their huge success on image classification, the number of images to mix has not been profoundly investigated by the previous works, only showing the naive K-image expansion leads to poor performance degradation. This paper derives a new K-image mixing augmentation based on the stick-breaking process under Dirichlet prior. We show that our method can train more robust and generalized classifiers through extensive experiments and analysis on classification accuracy, a shape of a loss landscape and adversarial robustness, than the usual two-image methods. Furthermore, we show that our probabilistic model can measure the sample-wise uncertainty and can boost the efficiency for Network Architecture Search (NAS) with 7x reduced search time.

Introduction

The importance of data augmentation becomes further emphasized after the advent of deep learning networks (DeVries and Taylor 2017; Yun et al. 2019; Zhang et al. 2017). Through employing the proper data augmentation, we can resolve both the performance degradation from insufficient data and the weak robustness to the noisy data (Chun et al. 2020). Inspired by the observations, many studies have proposed various augmentation methods for deep learning network.

Among the various data augmentation methods widely used, the image-mixing augmentation methods, especially CutMix (Yun et al. 2019), recently show the impressive performance to train the large-scaled deep learning networks. The image-mixing augmentation methods augment a new image by mixing the two paired images. For example, CutMix mixes the paired images by re-formulating their segments into one image. From the simple mechanism, the image-mixing augmentation successfully improves the performance of deep learning networks in various scenarios. Furthermore, with the image-mixing augmentation, the deep learning model can achieve the improved robustness to the corrupted and uncertain data.

However, study of the nature of the image-mixing augmentation is still not fully discovered. Specifically, even the optimal number of images to mix has not been profoundly

studied. In previous works (Kim et al. 2021; Zhang et al. 2017), there were *naive* attempts of K -image expansions of the augmentation reporting undesirable performance degradation and Zhang et al. (2017) empirically decided to select the number of images K as 2. Here, we aim to answer the following question: Does the $K = 2$ number of image is optimal for image-mixing augmentation?

We derive a novel formulation that can generalize the image-mixing augmentation. Based on the proposed formulation, we successfully obtain the improved results even after expanding various image-mixing augmentation methods. Especially, we find that the mixture of three or more images can further improve the performance of the baseline methods using only the paired images. The superiority of the generalized formulation is validated with various classification scenarios and analysis. In addition, we analyze the test robustness of our method, which confirms that our method can drive the model into widest (flattest) and deepest local minima among the comparisons. In terms of adversarial robustness, we experimentally found that image-mixing augmentation methods strengthen adversarial robustness, and the expansion into the K -image case further improves it.

Also, we show that the proposed image-mixing augmentation can be utilized to define uncertainty of the data samples. Based on the estimated uncertainty, we can acquire the subsampled data pool that can efficiently represent the overall data distribution. We show the efficiency of our subsampling framework by employing the proposed scheme on Network Architecture Search (NAS), preserving the performance with 7.7 times faster speed by utilizing the subsampled data pool as a training set.

Our contribution can be summarized as follows.

- We formulate the generalized version of the image-mixing augmentations for image classification, showing better generalization ability on unseen data against the baseline methods.
- We experimentally analyze the reason for the better generalization of K -image augmentation by illustrating a loss landscape near discovered minima. As a result, we show that it makes a model converge to a more wider and deeper local minima. In this regard, we also demonstrate that K -image augmentation improves adversarial robustness of the model.

^{*}These authors contributed equally.

- We propose a new data subsampling method by measuring sample uncertainty based on the proposed image-mixing augmentation, especially beneficial for handling the case having a small number of training samples. We further verify the efficiency of the proposed subsampling method by applying to NAS.

Related Works

Augmentation: Adding augmentation for training the classification network has become a new standard to achieve the high performance. Starting from the simple augmentations such as random crop, flipping, and color jittering, many others including Cutout (DeVries and Taylor 2017), Mixup (Zhang et al. 2017), CutMix (Yun et al. 2019), PuzzleMix (Kim, Choo, and Song 2020), SaliencyMix (Uddin et al. 2021), and Co-Mixup (Kim et al. 2021) have been proposed. Among the methods, the augmentations such as CutMix, Mixup, PuzzleMix and SaliencyMix usually mixed two images, and their recent variant, Co-Mixup, has further reported impressive performance enhancement in classification. Co-Mixup also generalized the image-mixing augmentation methods into K-image cases using submodular-supermodular optimization, which requires huge computational cost. However, our proposed K-image mixing augmentation methods do not require optimization process, showing less computational overhead and similar performance compared to Co-Mixup (Table 2). **Data Efficiency:** Regarding the efficient utilization of training dataset with a semantically important measure, several approaches have focused on collecting examples that are considered informative by re-weighting the importance of each training samples from various approaches: calculating the importance value from additional forward (Katharopoulos and Fleuret 2018) and backward path (Ren et al. 2018) of training, defining approximated function (Katharopoulos and Fleuret 2017), or using loss based training scheme (Freund and Schapire 1997; Malisiewicz, Gupta, and Efros 2011; Lin et al. 2017). Nevertheless, a criterion based on the hardness of example cannot be generalized in case of presence of samples that have label noise. Kumar, Packer, and Koller (2010) also showed that the hard examples are not preferred in initial stages of training, while easy examples are preferred. Following the intuitions of previous works towards measuring the importance of samples, we propose a robust importance subsampling methodology. Among the categories, we apply our subsampling concept to the differentiable search based NAS, showing strong points in both of search time and accuracy.

Main Method

In this section, we will define the formulation for the proposed K-image mixing augmentation and show the probabilistic framework of the augmentation on classification. Then, as a novel way to use K-image mixing augmentation, we will propose a subsampling method which utilizes the measured uncertainty of augmented data samples.

Formulation for K-image Mixing Augmentation

Here, we define the formulation for K-image generalization of image mixing augmentations on classification task. As



Figure 1: Example of three-image composition in CutMix case. We composite red box to green box, green box to blue box with the ratio of $1 : 1 - v_1$, and $1 : 1 - v_2$ as in (4). Consequently, the region proportion of each image fraction r_1 (red diagonal pattern), r_2 (green diagonal pattern), and r_3 (blue diagonal pattern) will correspond to $\{\phi_1, \phi_2, \phi_3\}$, which follows Dirichlet distribution.

sume that augmented sample x_c is composed of x_1, \dots, x_K , as in:

$$x_c = f_c(x_1, \dots, x_K; \phi_1, \dots, \phi_K), \quad (1)$$

where the function $f_c(\cdot)$ denotes the composite function, and the term $\phi = \{\phi_1, \dots, \phi_K\}$ is a mixing parameter denoting the portion of each sample x_k on the composite sample x_c . We note that it is a generalization of the popular image-mixing augmentations, CutMix (Yun et al. 2019) and Mixup (Zhang et al. 2017) using two images, to K-image case. Specifically, for the Mixup case which we name as *DMixup*, the function $f_c(\cdot)$ is defined by the weighted summation as:

$$x_c = \sum_{k=1}^K \phi_k x_k. \quad (2)$$

The mixing parameter ϕ is defined by Beta distribution in usual two-image cases (Yun et al. 2019; Zhang et al. 2017), and naturally be expanded to Dirichlet distribution $\phi \sim Dir(\alpha)$, $\alpha \in \mathbb{R}^K$. Obviously, the composite sample x_c is random variable given the hyper-parameter α .

K-image generalization of CutMix For K-image generalization of CutMix which we name as *DCutMix*, the definition of the function $f_c(\cdot)$ is more complicated since the function should contribute all the segments of images x_1, \dots, x_K to composite image x_c with respect to their mixing parameters ϕ . Here, we composite the images by the stick-breaking process (SBP, Sethuraman (1994)), one widely used approach of sampling from Dirichlet distribution.

Assume that we sample ϕ from the prior distribution $Dir(\alpha)$ and want to composite the image with respect to the proportion $\phi_k \in \phi$, $\sum_k \phi_k = 1$. From SBP, the composition can be done by defining the intermediate random variable $v = [v_1, \dots, v_{K-1}] \in \mathbb{R}^{K-1}$ such that:

$$v_1 = \phi_1$$

$$v_k = \phi_k / \prod_{j=1}^{k-1} (1 - v_j), \quad k = 2, \dots, K-1. \quad (3)$$

Note that the variable v is sampled from $Beta(1, \alpha)$ by the derivation of SBP. Now, we define the image fractions $r = \{r_1, \dots, r_K\}$ from K different images which constitute to a mixed sample $x \in \mathbb{R}^{W \times H \times C'}$. Let the function $\tilde{r} = d(x|v)$

randomly discriminate the image fractions $\tilde{r} : x \setminus \tilde{r}$ with the area ratio $v : 1 - v$, where the term $x \setminus \tilde{r}$ denotes the region of x excluding \tilde{r} . Consequently, we calculate the fractions r as:

$$r_k = d(x \setminus \sum_{j=0}^{k-1} r_j | v_k), \quad k = 1, \dots, K - 1. \quad (4)$$

where the virtual fraction r_0 is set to \emptyset , and the last fraction $r_K = x \setminus \sum_{j=1}^{K-1} r_j$. Figure 1 shows the example of the image composition. The discrimination function $d(\cdot)$ determines the exact bounding box coordinates $r_{k_x}, r_{k_y}, r_{k_w}, r_{k_h}$ of image fraction r_k through the uniform random variable γ to be located within the bounding box coordinates of former image patch r_{k-1} :

$$\begin{aligned} r_{k_x} &\sim \text{Unif}(r_{k-1_x}, r_{k-1_x} + r_{k-1_w} - r_{k_w}), \\ r_{k_y} &\sim \text{Unif}(r_{k-1_y}, r_{k-1_y} + r_{k-1_h} - r_{k_h}) \end{aligned} \quad (5)$$

where its width (r_{k_w}) and height (r_{k_h}) are determined by v_k as defined in (4). Note that for $k = 1$ case, $r_{1_x} = 0, r_{1_y} = 0, r_{1_w} = W$ and $r_{1_h} = H$. Hence, the composite function f_c of the DCutMix will be governed by hyper-parameter α and random variable γ . Full pseudo code of DCutMix training algorithm is presented in Supplementary Materials (SM).

In the subsequent Experiment section, we will experimentally show the advantage of the proposed K-image generalization in terms of loss landscape, adversarial robustness, and classification accuracy.

Probabilistic framework The overall probabilistic framework of the classification problem with applying the proposed augmentation, is defined as:

$$\begin{aligned} p(l_c | x_c) &= \int p(l_c | x_c, \phi) p(\phi | \alpha) d\phi, \\ &= \int p(\sum_k \{\phi_k l_k\} | f_c(\mathbf{x}; \phi)) p(\phi | \alpha) d\phi, \\ &\cong \frac{1}{N_s} \sum_{\phi^{(j)}} f_W(\{\sum_k \phi_k^{(j)} l_k\} | f_c(\mathbf{x}; \phi^{(j)})), \end{aligned} \quad (6)$$

where $(\mathbf{x}, \mathbf{l}) = \{(x_1, l_1), \dots, (x_K, l_K)\}, l_c = \sum_k \{\phi_k l_k\}$, and $\phi^{(j)}$ is the j^{th} sample drawn from the Dirichlet prior distribution $p(\cdot | \alpha)$. Hereafter, we define the label $l_i \in \mathbb{R}^C$ to be a one-hot indexing variable denoting one of total C classes. Based on the derivation from Monte-Carlo Dropout (Gal and Ghahramani 2016), we can approximate the distribution $p(l_c | x_c)$ to the variational function $f_W(\cdot)$ with regard to several different ϕ and γ samples, which is realized by a classification network having the network parameter W with softmax output. For DCutMix case, we consider another variable γ in (6) as:

$$p(l_c | x_c) \cong \sum_{\gamma^{(i)}} \sum_{\phi^{(j)}} f_W(\{\sum_k \phi_k^{(j)} l_k\} | f_c(\mathbf{x}; \phi^{(j)}, \gamma^{(i)})). \quad (7)$$

Consequently, by (6) and (7), we can approximately infer the posterior $p(l_c | x_c)$ by estimating the predictive mean of network outputs depending on several differently augmented data samples from various ϕ and γ samples. Similarly, the uncertainty of a data sample can be approximated by variously augmented data samples.

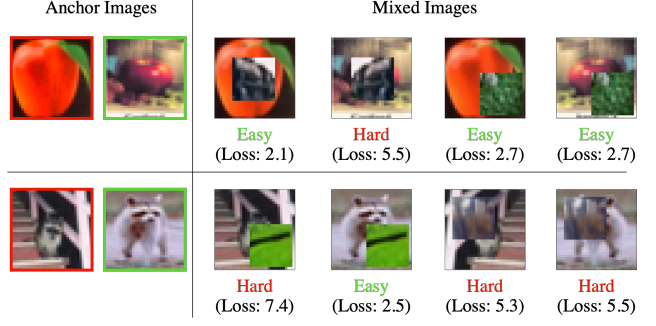


Figure 2: Example of composite samples where the loss values are highly variable or invariable depending on the position of occlusion by non-anchor image patches. The anchor images (bordered with green) have highly variable loss values depending on the occlusion, while the other anchor images (bordered with red) have relatively invariable loss values regardless of the occlusion.

Subsampling using the Measured Data Uncertainty

As a new way to utilize the K-image mixing augmentation, we propose a subsampling method which takes into account the data uncertainty obtained from K-image augmentation for the first time. In order to measure the uncertainty of a data sample, we define the loss distribution $L(l_c | x_c)$ for variously augmented data samples depending on ϕ, γ and its expectation can be approximated based on (7) as:

$$\mathbb{E}[L(l_c | x_c)] \cong \sum_{\gamma^{(i)}} \sum_{\phi^{(j)}} \mathcal{L}(\{\sum_k \phi_k^{(j)} l_k\} | f_c(\mathbf{x}; \phi^{(j)}, \gamma^{(i)})), \quad (8)$$

where $\mathbf{x} = \{x_1, \dots, x_K\}$, and \mathcal{L} denotes the cross-entropy loss. The expectation is defined on the space by the random variable ϕ and γ . In a similar manner, the uncertainty can also be acquired by estimating variance of the loss distribution L . Figure 2 shows the qualitative example of uncertainty measuring given sample data and its mixed images. From the example, we can see the diverse tendency of loss values changes for each mixed image, mainly depending on the randomly selected position of occlusion caused by non-anchor image patches.

For measuring the sample-wise uncertainty using the loss distribution, we select an *anchor sample* $x_i \in \mathbf{x}$ with fixed ϕ_i and then jitter $\phi \setminus \phi_i$ related to other non-anchor samples $\mathbf{x} \setminus x_i$ to calculate the uncertainty of the anchor sample x_i . The $\phi \setminus \phi_i$ are drawn from a conditional Dirichlet distribution $D(\alpha | \alpha_i)$, by its definition. We will term $L_i = \{L_{i,m} | m = 1, \dots, M\}$ as the loss distribution for all the mixed images given the anchor x_i where the loss is correspondingly calculated by (8). The number M denotes the total number of sampling $\phi \setminus \phi_i$ from $D(\alpha | \alpha_i)$.

Based on the sample-wise uncertainty measurement, we target to sample core training data sub-set among the entire training dataset. We suppose that for better generalization of a neural network under training with small number of data points and image-mixing augmentation, the core training sub-set should consist of the highly uncertain samples which can serve as both easy- and hard-level samples depending on

| Model | # Params | Top-1 Err (%) |
|---|----------|----------------------|
| PyramidNet-110 ($\tilde{\alpha} = 64$) (Han, Kim, and Kim 2017) | 1.7 M | 19.85 |
| + Mixup (Zhang et al. 2017) | 1.7 M | 18.92 (-0.93) |
| + CutMix (Yun et al. 2019) | 1.7 M | 17.97 (-1.88) |
| + DMixup ($K = 3, \alpha = \frac{1}{3}$) | 1.7 M | 18.60 (-1.25) |
| + DCutMix ($K = 5, \alpha = 0.2$) | 1.7 M | 16.95 (-2.90) |
| PyramidNet-200 ($\tilde{\alpha} = 240$) | 26.8 M | 16.45 |
| + StochDepth (Huang et al. 2016) | 26.8 M | 15.86 (-0.59) |
| + Label Smoothing (Szegedy et al. 2016) | 26.8 M | 16.73 (+0.28) |
| + Cutout (DeVries and Taylor 2017) | 26.8 M | 16.53 (+0.08) |
| + DropBlock (Ghiasi, Lin, and Le 2018) | 26.8 M | 15.73 (-0.72) |
| + Mixup (Zhang et al. 2017) | 26.8 M | 15.63 (-0.82) |
| + Manifold Mixup (Verma et al. 2019) | 26.8 M | 15.09 (-1.36) |
| + CutMix (Yun et al. 2019) | 26.8 M | 14.47 (-1.98) |
| + DMixup ($K = 3, \alpha = 1$) | 26.8 M | 15.07 (-1.38) |
| + DCutMix ($K = 5, \alpha = 1$) | 26.8 M | 13.86 (-2.59) |

| Model | Top-1 Err (%) |
|--|---------------------|
| PyramidNet-200 ($\tilde{\alpha} = 240$) | 3.85 |
| PyramidNet-200 + Cutout (DeVries and Taylor 2017) | 3.10 (-0.75) |
| PyramidNet-200 + Mixup (Zhang et al. 2017) | 3.09 (-0.76) |
| PyramidNet-200 + Manifold Mixup (Verma et al. 2019) | 3.15 (-0.7) |
| PyramidNet-200 + CutMix (Yun et al. 2019) | 2.88 (-0.97) |
| PyramidNet-200 + DMixup ($K = 5, \alpha = 0.2$) | 2.90 (-0.95) |
| PyramidNet-200 + DCutMix ($K = 3, \alpha = \frac{1}{3}$) | 2.42 (-1.43) |

Table 1: Comparison of DCutMix and DMixup against other augmentations and regularization methods for PyramidNet-110, 200 models on CIFAR-100 dataset (top) and CIFAR-10 dataset (bottom). The values in the parentheses of top-1 error denote error rate reduction compared to the vanilla model where no augmentation or regularization was applied.

the image-mixing augmentation (e.g. the images bordered with green in Figure 2). Therefore, a new training subset is subsampled by descending order of uncertainty measure (See SM for detailed procedure). We observed that employing coefficient of variation (CV) metric, which is defined as $\frac{\sigma(L_i)}{m(L_i)}$ where $\sigma(\cdot)$ and $m(\cdot)$ is the standard deviation and average of L_i , is most effective for measuring the uncertainty (See Figure 4a for details).

Experiments and Discussion

Here, we experimentally verify effect of the K-expanded image mixing augmentation. Firstly, on CIFAR-10/100, we show the improved classification performance after applying our method and analyze the advantage of it in terms of the shape of the loss landscape. Secondly, on ImageNet, we propose a more elaborately designed K-image mixing augmentation which considers saliency map for overcoming a label noise issue, and show the experimental result on classification and adversarial robustness for further discussion. Finally, we demonstrate effectiveness of proposed data subsampling method and its practical application on NAS.

Experimental Result on Image Classification

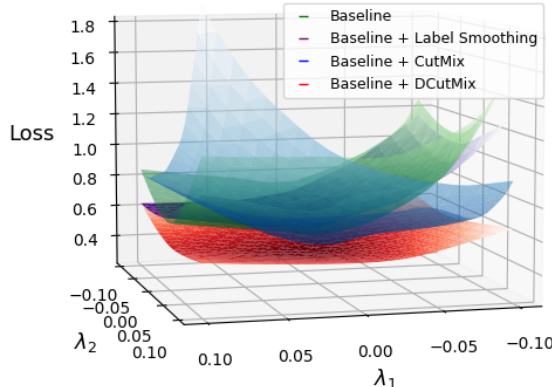
CIFAR-10/100 We present classification test results on CIFAR-10 and 100 (Krizhevsky, Hinton et al. 2009) datasets in Table 1. The results are obtained from the equivalent training and augmentation specific hyper-parameter setup used

in Yun et al. (2019). Firstly, Table 1 (top) shows the superiority of DCutMix and DMixup over the other augmentation and regularization methods on CIFAR-100 dataset. With light-weight backbone PyramidNet-110 (Han, Kim, and Kim 2017), DCutMix and DMixup improve the performance compared to the baselines (i.e. CutMix and Mixup) by approximately 1% and 0.32%, respectively. For the deeper neural network PyramidNet-200, DCutMix and DMixup achieve the enhancement compared to the baselines and DCutMix shows the lowest top-1 error compared to other baselines. Secondly, we evaluate our proposed methods on CIFAR-10 dataset as shown in Table 1 (bottom). We again observe that DCutMix and DMixup both achieved the performance enhancement. Specifically, DCutMix shows the best performance among the baseline augmentation methods again. Finally, we further compare our DCutMix and DMixup with state-of-the-art image-mixing augmentation methods in Table 2. DCutMix achieved not only better accuracy than PuzzleMix (Kim, Choo, and Song 2020) but also a competitive accuracy compared to the Co-Mixup (Kim et al. 2021). Note that Co-Mixup has much more training time overhead (about 27 times) than ours due to the high optimization cost. These overall results demonstrate effectiveness of the proposed K-image generalization for augmentation methods.

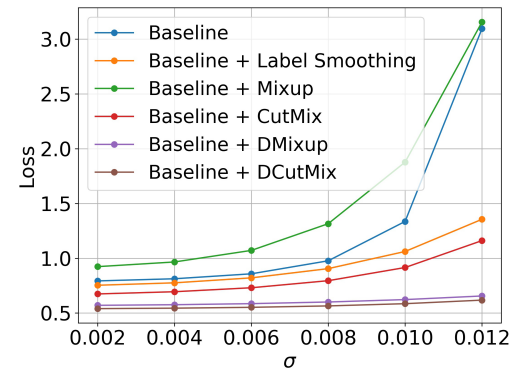
Analysis on the shape of the loss landscape For more explicit investigation, we analyze DCutMix with its loss landscape. Flatness of the loss landscape near local minima has been considered as one key signal for achieving better generalization of the model in various situations, by the number of previous studies (Keskar et al. 2016; Pereyra et al. 2017; Zhang et al. 2018; Chaudhari et al. 2019; Cha et al. 2020). The general interpretation on the shape of the loss landscape is that if a model converges to a wide (flat) local minima, the model tends to have better generalization performance on unseen test dataset.

Based on these findings, we plot the patterns of loss landscapes of each model using PyHessian (Yao et al. 2019) framework, as shown in Figure 3a. The details of plotting the loss landscape with PyHessian is described in SM. The plotted result shows that DCutMix has a wider loss landscape near local minima among the comparisons. Also, DCutMix has lower losses in overall, denoting well generalization to the unseen test data as well (See Figure 1 in the SM for additional comparison of Mixup with DMixup). In Figure 3b, we further plotted the patterns of loss landscape for each model by perturbing the model parameters with random Gaussian noise with increasing its degree of variance σ (Zhang et al. 2018). DCutMix and DMixup clearly shows the most widest and lowest loss landscape compared to the other methods including the baseline two-image mixing augmentations, such as CutMix and Mixup. Especially for DMixup, we observe that it largely strengthens the convergence stability of Mixup. We believe that this observation can be one signal for interpreting the superiority of proposed K-image mixing augmentation.

From a more analytical point of view, we can hypothesize that the merit of K-image generalization of CutMix and Mixup regarding the wide flat local minima comes from a more softened label than that of CutMix and Mixup. Several



(a) 3-d loss surface plot by perturbing the model across the two directions using PyHessian.



(b) 2-d loss surface plot by perturbing the model across the one random direction.

Figure 3: Comparison of image mixing augmentation and regularization methods in perspective of the loss-surface near local minima. We measured the loss-surfaces on test set of CIFAR-100 with PyramidNet (Han, Kim, and Kim 2017).

| Model | Vanilla | Mixup | CutMix | PuzzleMix | Co-Mixup | DMixup (ours) | DCutMix (ours) |
|-------|------------|---------------|---------------|---------------|----------------|----------------------|----------------------|
| a | 23.59 (1x) | 22.43 (1.04x) | 21.29 (1.1x) | 20.62 (2.73x) | 19.87 (29.34x) | 21.68 (1.14x) | 20.50 (1.07x) |
| b | 21.70 (1x) | 20.08 (1.02x) | 20.55 (1.04x) | 19.24 (2.25x) | 19.15 (13.46x) | 19.13 (1.02x) | 18.64 (1.01x) |
| c | 21.79 (1x) | 21.70 (1.02x) | 22.28 (1.05x) | 21.12 (2.22x) | 19.78 (6.93x) | 20.09 (1.02x) | 20.48 (1.02x) |

Table 2: Comparison of Top-1 error rate and training time for the state-of-the-art image mixing augmentations on CIFAR-100 with various backbone models. (a): PreActResNet18 (He et al. 2016), (b): WRN16-8 (Zagoruyko and Komodakis 2016), (c): ResNeXt29-4-24 (Xie et al. 2017). Values in the parentheses denote ratio of average training time relative to the baseline (vanilla) case.

papers have reported that a model trained with an *artificially* smoothed label can make the model converge to wide local minima and hence achieve better generalization (Pereyra et al. 2017; Zhang et al. 2018; Cha et al. 2020), *i.e.*, the superior result of Label Smoothing (Pereyra et al. 2017) compared to the baseline in Figure 3a and Figure 3b. However, as opposed to the previous regularization methods using *artificially* smoothed label, note that our softened label *directly* reveals the augmented ratio of several images, and hence, we conjecture that this can be a key factor why the model trained by our approach converges to lower and wider local minima.

ImageNet We present ImageNet classification results of DCutMix and DMixup compared to the two-image mixing baselines: CutMix and Mixup. The results are obtained under the equivalent training and augmentation specific hyper-parameter setup used in Yun et al. (2019). In Table 3 (top), DMixup considerably improved performance of Mixup and Manifold Mixup by 0.7% and 0.62% reduced top-1 error, respectively. However, DCutMix showed higher top-1 error rate compared to CutMix. We analyzed the cause of this result; we found out that DCutMix suffers from the label noise issue where a background object other than ground truth class object is contained in the randomly cropped image (Yun et al. 2021), as shown in Figure 2 of SM. Table 3 (bottom) shows that as the number of mixing images K increases, performance of DCutMix is significantly deteriorated due to high possibility of background objects being accumulated K times. In order to address such label noise issue, we devised a more sophisticated mixing method, named as Saliency-DCutMix,

which employs saliency-map information to be integrated with our DCutMix (the detailed description of it is proposed in the SM). In Table 3 (bottom), Saliency-DCutMix indeed shows relatively stable and significantly improved performance regardless of K compared to DCutMix. Furthermore, Saliency-DCutMix showed higher performance than its baseline two-image mixing augmentation method, CutMix, as shown in Table 3 (top).

Adversarial robustness After the vulnerability of deep neural networks was revealed by Szegedy et al. (2013), achieving not only a superior classification performance for non-attacked examples (standard accuracy) but also adversarial robustness (robust accuracy) has been considered as the key factor to make the deep neural network truly robust and reliable (Goodfellow, Shlens, and Szegedy 2014; Madry et al. 2017; Guo et al. 2017; Dong et al. 2020). For achieving higher adversarial robustness, several attack and defense methods have been proposed alternately as if competing with each other (Goodfellow, Shlens, and Szegedy 2014; Madry et al. 2017; Guo et al. 2017; Dong et al. 2020). On the other side, Madry et al. (2017); Yun et al. (2019) have reported that training a model with an input transformation or augmentation enhances robustness of the model against adversarial examples without adversarial training (Madry et al. 2017) which suffers from a huge training cost and a serious trade-off between standard and robust accuracy.

In this section, we demonstrate the additional advantage of K-image mixing augmentation in terms of adversarial robustness. We selected each of a classification model (ResNet-50)

| Model | Top-1 Err (%) | Top-5 Err (%) | | |
|--|------------------|------------------|------------------|------------------|
| ResNet-50 (Baseline) | 23.68 | 7.05 | | |
| ResNet-50 + Mixup | 22.58 | 6.40 | | |
| ResNet-50 + Manifold Mixup | 22.50 | 6.21 | | |
| ResNet-50 + CutMix | 21.40 | 5.92 | | |
| ResNet-50 + DMixup ($K = 3, \alpha = \frac{1}{3}$) | 21.88 | 6.15 | | |
| ResNet-50 + DCutMix ($K = 3, \alpha = \frac{1}{3}$) | 21.76 | 5.91 | | |
| ResNet-50 + Saliency-DCutMix ($K = 3, \alpha = \frac{1}{3}$) | 21.38 | 5.87 | | |
| Method | α | K | Top-1 Err (%) | Top-5 Err (%) |
| ResNet-50 + DCutMix | 1 | 3 | 21.62 | 5.92 |
| ResNet-50 + DCutMix | 1 | 4 | 22.17 | 6.23 |
| ResNet-50 + DCutMix | 1 | 5 | 22.02 | 6.05 |
| ResNet-50 + DCutMix | 1 | 7 | 22.39 | 6.17 |
| ResNet-50 + DCutMix | 1 | 9 | 22.58 | 6.34 |
| ResNet-50 + Saliency-DCutMix | 1 | 3 | 21.40 | 5.87 |
| ResNet-50 + Saliency-DCutMix | 1 | 4 | 21.55 | 6.00 |
| ResNet-50 + Saliency-DCutMix | 1 | 5 | 21.70 | 5.93 |
| ResNet-50 + Saliency-DCutMix | 1 | 7 | 21.44 | 5.93 |

Table 3: Performance of DMixup and DCutMix, and Saliency-DCutMix on ImageNet (top). Impact of K on DCutMix and Saliency-DCutMix (bottom).

trained by Baseline (w/o augmentation), CutMix, DCutMix and Saliency-DCutMix using ImageNet training dataset. To evaluate adversarial robustness against more diverse types of attack, we consider not only white-box attack as in Yun et al. (2019), but also gray- and black-box attack (Guo et al. 2017). The detailed experimental settings for adversarial attack are proposed in the SM. Table 4 shows top-1 accuracy on given adversarial examples generated by each attack. As also proposed in Yun et al. (2019), the model trained with CutMix shows better adversarial robustness compared to the Baseline case against all types of attack. DCutMix achieves more improved adversarial robustness against gray- and black-box attacks compared to CutMix, however, it was not against white-box attack. Note that white-box attack is the most powerful attack among three types of attack. In this point, we hypothesized that the label noise issue of DCutMix causes degradation of adversarial robustness against the strong attack (white-box), and this hypothesis was indirectly confirmed through experiments on Saliency-DCutMix. We clearly observe that saliency map guided DCutmix (Saliency-DCutmix) further strengthens adversarial robustness over both CutMix and DCutMix against all types of attack.

For more sophisticated investigation of robustness towards input data distribution shift, we evaluated accuracy of augmentation methods on ImageNet-A dataset (Hendrycks et al. 2021). ImageNet-A contains natural adversarial examples which cause an ImageNet-pretrained model to wrongly classify without any adversarial attacks. In Table 4, we found that performance tendency on ImageNet-A is similar to that of adversarially attacked ImageNet; CutMix showed better accuracy compared to Baseline and DCutMix case. Meanwhile, Saliency-DCutMix further improved accuracy of CutMix, showing better generalization on natural adversarial examples and hence better robustness on input data distribution shift.

| Model | White-box | Gray-box | Black-box | ImageNet-A |
|---|--------------------------------------|-------------------------------------|-------------------------------------|--------------|
| | FGSM ($L_\infty, \epsilon = 8$) | PGD ($L_\infty, \epsilon = 8$) | PGD ($L_\infty, \epsilon = 8$) | |
| ResNet-50 (Baseline) | 14.34 | 40.74 | 46.01 | 3.38 |
| + CutMix | 40.89 (+26.55) | 43.38 (+2.64) | 51.06 (+5.05) | 7.46 (+4.08) |
| + DCutMix ($K = 3, \alpha = \frac{1}{3}$) | 32.90 (+18.56) | 43.63 (+2.89) | 51.73 (+5.72) | 5.84 (+2.46) |
| + Saliency-DCutMix ($K = 3, \alpha = \frac{1}{3}$) | 41.37 (+27.03) | 44.27 (+3.53) | 51.91 (+5.90) | 7.69 (+4.31) |

Table 4: Top-1 robust accuracy on ImageNet against various adversarial attacks (2nd, 3rd, 4th column) and accuracy on ImageNet-A (last column). The values in parentheses denote accuracy increment compared to the Baseline case.

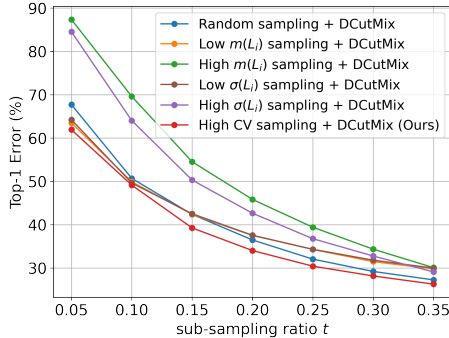
We also tested robustness towards the out-of-distribution (OOD) samples with ImageNet-O dataset (Hendrycks et al. 2021), where we found that augmentation techniques hardly strengthen robustness towards OOD examples (See Table 3 in SM), as reported in Hendrycks et al. (2021).

Data Subsampling and Application

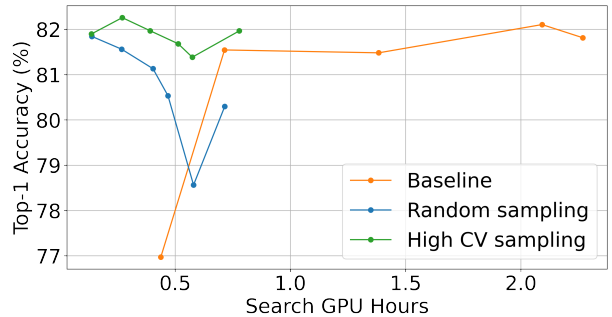
Data Subsampling We investigate the effect of the proposed subsampling method when trained with DCutMix as an augmentation in Figure 4a. In the figure, we compare our data subsampling method with others using various subsampling measures. For all subsequent experiments with regard to data subsampling, full 10K validation set of CIFAR-100 was used for evaluation, and we report the averaged results by three independent random seeds using PyramidNet (Han, Kim, and Kim 2017).

As shown in Figure 4a, sampling the easy-only or hard-only examples based on $m(L_i)$ shows deteriorated performance compared to the random subsampling. The hard-only subsampling severely suffered from poor generalization. This result indicates that subsampling only hard samples where the salient regions were occluded by image-mixing augmentation being applied (see Figure 2) is not desirable under the constraint of small number of training samples. In a similar manner, subsampling only easy samples extracts the biased data samples that cannot be helpful for better generalization. Also, simply employing standard deviation $\sigma(L_i)$ as subsampling measure showed a similar test error plot compared to the above mean based sampling methods. On the other hand, our high CV based subsampling outperforms the random sampling by a significant margin, especially 5.79% lower test error in case of the number of subsampled training samples being extremely small (i.e. $t = 0.05$). High CV subsampling enables to acquire various levels of data samples from easy to hard, since it basically selects the easy data samples which can also frequently become hard samples depending on the image-mixing augmentation. Therefore, High CV subsampling leads to better performance when training with image-mixing augmentation. Moreover, we clearly observed superiority of our subsampling method over the other subsampling methods employing uncertainty derived by weight dropout (Gal, Islam, and Ghahramani 2017) and *K-Center Coreset* sampling method (Sener and Savarese 2017), as shown in Figure 4 of SM. Additional ablation studies of our subsampling method are presented in Figure 3 of SM.

Application on NAS We further show the practical and effective usage of our proposed data subsampling method on



(a) Top-1 error plotting for data subsampling methods. t denotes ratio of images in subsampled set to those in whole training set.



(b) Top-1 accuracy plotting of NAS given GPU searching cost on CIFAR-100.

Figure 4: Experiments on data subsampling: performance of various data subsampling methods (a). The graph (b) shows the speedup of NAS from the proposed subsampling method: searching on entire CIFAR-100 dataset (Baseline), on randomly subsampled CIFAR-100, and on subsampled CIFAR-100 by high CV measure.

| Architecture | Top-1 Err (%) | Top-5 Err (%) | # Params (M) | # FLOPs (M) | Search Cost (GPU days) | Search method |
|---|---------------|---------------|--------------|-------------|------------------------|----------------|
| AmoebaNet-C (Real et al. 2019) | 24.3 | 7.6 | 6.4 | 570 | 3150 | evolution |
| MnasNet-92 (Tan et al. 2019) | 25.2 | 8.0 | 4.4 | 388 | - | RL |
| ProxylessNAS (Cai, Zhu, and Han 2018) | 24.9 | 7.5 | 7.1 | 465 | 8.3 | gradient-based |
| SNAS (Xie et al. 2018) | 27.3 | 9.2 | 4.3 | 522 | 1.5 | gradient-based |
| BayesNAS (Zhou et al. 2019) | 26.5 | 8.9 | 3.9 | - | 0.2 | gradient-based |
| PC-DARTS (CIFAR10) (Xu et al. 2019) | 25.1 | 7.8 | 5.3 | 586 | 0.1 | gradient-based |
| PC-DARTS (ImageNet) (Xu et al. 2019) | 24.2 | 7.3 | 5.3 | 597 | 3.8 | gradient-based |
| PC-DARTS (CIFAR100) (Xu et al. 2019) | 23.8 | 7.09 | 6.3 | 730 | 0.1 | gradient-based |
| PC-DARTS (High CV Sub-sampled CIFAR100) | 24.3 | 7.2 | 5.8 | 671 | 0.01 | gradient-based |

Table 5: Comparison of the state-of-the-art NAS methods on ImageNet under comparably small resource constraints. (·) denotes the proxy dataset where the architecture was searched on.

another domain, specifically on network architecture search (NAS). Our goal is to reduce the time spent for searching the architectures by searching on the subsampled dataset drawn from our framework, rather than on the full training dataset. We adopt one of the most computationally efficient and stabilized NAS method, PC-DARTS (Xu et al. 2019) as our baseline. Here, we used the equivalent searching hyper-parameters proposed in Xu et al. (2019) (See SM for details).

In Figure 4b, we plotted the performance of neural networks searched on the entire CIFAR-100 dataset (baseline) by adjusting the searching epochs, while adjusting the sub-sampling ratio t for searching on the randomly subsampled dataset and our subsampled dataset drawn by high CV measure. The result shows the outstanding efficiency of our sub-sampling framework in terms of search time and accuracy. Especially, ours (searching on high CV subsampled dataset) achieves comparable accuracy with $7.7 \times$ reduced search time compared to other baselines. Furthermore, ours consistently outperforms random subsampling given the equivalent number of data samples for searching.

As shown in Table 5, we could observe that ours serves as an effective proxy dataset and the neural network searched by ours is also well-generalized on ImageNet. Note that, ours reduced search GPU time up to 0.01 days (i.e. 16 minutes), while showing comparable or even higher accuracy compared to the models searched with PC-DARTS on the entire CIFAR-

10, CIFAR-100, and randomly subsampled ImageNet dataset. Also, compared to the other NAS methods, ours achieves the best accuracy performance while enjoying the significantly reduced search computational cost.

Concluding Remarks

In this paper, we presented the advantage of the expanding the number of images for the image-mixing augmentation based on various experimental results and analysis. First, we proposed the generalized method for K-image mixing augmentation motivated by the stick-breaking process (SBP). Second, we showed the proposed K-image mixing augmentation improves classification performance and, from a novel perspective, we analyzed the key factor of this improvement comes from converging to a wide local minima. Also, we empirically found that increasing the number of images for the image mixing augmentation enhances adversarial robustness of a classification model against various types of adversarial examples. Additionally, we derived the new subsampling method which utilizes the proposed K-image mixing augmentation in the novel way and we experimentally observe that the proposed subsampling method can effectively reduce search time without performance degradation. We hope our observations and analyses can lead to new research directions for the image mixing augmentation and data subsampling.

References

Cai, H.; Zhu, L.; and Han, S. 2018. Proxylessnas: Direct neural architecture search on target task and hardware. [arXiv preprint arXiv:1812.00332](#).

Cha, S.; Hsu, H.; Calmon, F. P.; and Moon, T. 2020. CPR: Classifier-Projection Regularization for Continual Learning. [arXiv preprint arXiv:2006.07326](#).

Chaudhari, P.; Choromanska, A.; Soatto, S.; LeCun, Y.; Baldassi, C.; Borgs, C.; Chayes, J.; Sagun, L.; and Zecchina, R. 2019. Entropy-sgd: Biasing gradient descent into wide valleys. *Journal of Statistical Mechanics: Theory and Experiment*, 2019(12): 124018.

Chun, S.; Oh, S. J.; Yun, S.; Han, D.; Choe, J.; and Yoo, Y. 2020. An empirical evaluation on robustness and uncertainty of regularization methods. [arXiv preprint arXiv:2003.03879](#).

DeVries, T.; and Taylor, G. W. 2017. Improved regularization of convolutional neural networks with cutout. [arXiv preprint arXiv:1708.04552](#).

Dong, Y.; Fu, Q.-A.; Yang, X.; Pang, T.; Su, H.; Xiao, Z.; and Zhu, J. 2020. Benchmarking adversarial robustness on image classification. In *Proceedings of the IEEE/CVF Conference on Computer Vision and Pattern Recognition*, 321–331.

Freund, Y.; and Schapire, R. E. 1997. A decision-theoretic generalization of on-line learning and an application to boosting. *Journal of computer and system sciences*, 55(1): 119–139.

Gal, Y.; and Ghahramani, Z. 2016. Dropout as a bayesian approximation: Representing model uncertainty in deep learning. In *international conference on machine learning*, 1050–1059. PMLR.

Gal, Y.; Islam, R.; and Ghahramani, Z. 2017. Deep bayesian active learning with image data. In *International Conference on Machine Learning*, 1183–1192. PMLR.

Ghiasi, G.; Lin, T.-Y.; and Le, Q. V. 2018. DropBlock: A regularization method for convolutional networks. In *Advances in Neural Information Processing Systems*, 10750–10760.

Goodfellow, I. J.; Shlens, J.; and Szegedy, C. 2014. Explaining and harnessing adversarial examples. [arXiv preprint arXiv:1412.6572](#).

Guo, C.; Rana, M.; Cisse, M.; and Van Der Maaten, L. 2017. Countering adversarial images using input transformations. [arXiv preprint arXiv:1711.00117](#).

Han, D.; Kim, J.; and Kim, J. 2017. Deep pyramidal residual networks. In *Proceedings of the IEEE conference on computer vision and pattern recognition*, 5927–5935.

He, K.; Zhang, X.; Ren, S.; and Sun, J. 2016. Identity mappings in deep residual networks. In *European conference on computer vision*, 630–645. Springer.

Hendrycks, D.; Zhao, K.; Basart, S.; Steinhardt, J.; and Song, D. 2021. Natural adversarial examples. In *Proceedings of the IEEE/CVF Conference on Computer Vision and Pattern Recognition*, 15262–15271.

Huang, G.; Sun, Y.; Liu, Z.; Sedra, D.; and Weinberger, K. 2016. Deep networks with stochastic depth. In *ECCV*.

Katharopoulos, A.; and Fleuret, F. 2017. Biased importance sampling for deep neural network training. [arXiv preprint arXiv:1706.00043](#).

Katharopoulos, A.; and Fleuret, F. 2018. Not all samples are created equal: Deep learning with importance sampling. [arXiv preprint arXiv:1803.00942](#).

Keskar, N. S.; Mudigere, D.; Nocedal, J.; Smelyanskiy, M.; and Tang, P. T. P. 2016. On large-batch training for deep learning: Generalization gap and sharp minima. [arXiv preprint arXiv:1609.04836](#).

Kim, J.; Choo, W.; Jeong, H.; and Song, H. O. 2021. Co-Mixup: Saliency Guided Joint Mixup with Supermodular Diversity. In *International Conference on Learning Representations*.

Kim, J.-H.; Choo, W.; and Song, H. O. 2020. Puzzle mix: Exploiting saliency and local statistics for optimal mixup. In *International Conference on Machine Learning*, 5275–5285. PMLR.

Krizhevsky, A.; Hinton, G.; et al. 2009. Learning multiple layers of features from tiny images.

Kumar, M. P.; Packer, B.; and Koller, D. 2010. Self-paced learning for latent variable models. In *Advances in neural information processing systems*, 1189–1197.

Lin, T.-Y.; Goyal, P.; Girshick, R.; He, K.; and Dollár, P. 2017. Focal loss for dense object detection. In *Proceedings of the IEEE international conference on computer vision*, 2980–2988.

Madry, A.; Makelov, A.; Schmidt, L.; Tsipras, D.; and Vladu, A. 2017. Towards deep learning models resistant to adversarial attacks. [arXiv preprint arXiv:1706.06083](#).

Malisiewicz, T.; Gupta, A.; and Efros, A. A. 2011. Ensemble of exemplar-svms for object detection and beyond. In *2011 International conference on computer vision*, 89–96. IEEE.

Pereyra, G.; Tucker, G.; Chorowski, J.; Kaiser, Ł.; and Hinton, G. 2017. Regularizing neural networks by penalizing confident output distributions. [arXiv preprint arXiv:1701.06548](#).

Real, E.; Aggarwal, A.; Huang, Y.; and Le, Q. V. 2019. Regularized evolution for image classifier architecture search. In *AAAI*.

Ren, M.; Zeng, W.; Yang, B.; and Urtasun, R. 2018. Learning to reweight examples for robust deep learning. [arXiv preprint arXiv:1803.09050](#).

Sener, O.; and Savarese, S. 2017. Active learning for convolutional neural networks: A core-set approach. [arXiv preprint arXiv:1708.00489](#).

Sethuraman, J. 1994. A constructive definition of Dirichlet priors. *Statistica sinica*, 639–650.

Szegedy, C.; Vanhoucke, V.; Ioffe, S.; Shlens, J.; and Wojna, Z. 2016. Rethinking the inception architecture for computer vision. In *Proceedings of the IEEE conference on computer vision and pattern recognition*, 2818–2826.

Szegedy, C.; Zaremba, W.; Sutskever, I.; Bruna, J.; Erhan, D.; Goodfellow, I.; and Fergus, R. 2013. Intriguing properties of neural networks. [arXiv preprint arXiv:1312.6199](#).

Tan, M.; Chen, B.; Pang, R.; Vasudevan, V.; and Le, Q. V. 2019. MnasNet: Platform-aware neural architecture search for mobile. *CVPR*.

Uddin, A. F. M. S.; Monira, M. S.; Shin, W.; Chung, T.; and Bae, S.-H. 2021. SaliencyMix: A Saliency Guided Data Augmentation Strategy for Better Regularization. In *International Conference on Learning Representations*.

Verma, V.; Lamb, A.; Beckham, C.; Najafi, A.; Mitliagkas, I.; Lopez-Paz, D.; and Bengio, Y. 2019. Manifold Mixup: Better Representations by Interpolating Hidden States. In *International Conference on Machine Learning*, 6438–6447.

Xie, S.; Girshick, R.; Dollár, P.; Tu, Z.; and He, K. 2017. Aggregated residual transformations for deep neural networks. In *Proceedings of the IEEE conference on computer vision and pattern recognition*, 1492–1500.

Xie, S.; Zheng, H.; Liu, C.; and Lin, L. 2018. SNAS: stochastic neural architecture search. *arXiv preprint arXiv:1812.09926*.

Xu, Y.; Xie, L.; Zhang, X.; Chen, X.; Qi, G.-J.; Tian, Q.; and Xiong, H. 2019. Pcdarts: Partial channel connections for memory-efficient architecture search. In *International Conference on Learning Representations*.

Yao, Z.; Gholami, A.; Keutzer, K.; and Mahoney, M. 2019. PyHessian: Neural networks through the lens of the Hessian. *arXiv preprint arXiv:1912.07145*.

Yun, S.; Han, D.; Oh, S. J.; Chun, S.; Choe, J.; and Yoo, Y. 2019. Cutmix: Regularization strategy to train strong classifiers with localizable features. In *Proceedings of the IEEE International Conference on Computer Vision*, 6023–6032.

Yun, S.; Oh, S. J.; Heo, B.; Han, D.; Choe, J.; and Chun, S. 2021. Re-labeling imagenet: from single to multi-labels, from global to localized labels. In *Proceedings of the IEEE/CVF Conference on Computer Vision and Pattern Recognition*, 2340–2350.

Zagoruyko, S.; and Komodakis, N. 2016. Wide residual networks. *arXiv preprint arXiv:1605.07146*.

Zhang, H.; Cisse, M.; Dauphin, Y. N.; and Lopez-Paz, D. 2017. mixup: Beyond empirical risk minimization. *arXiv preprint arXiv:1710.09412*.

Zhang, Y.; Xiang, T.; Hospedales, T. M.; and Lu, H. 2018. Deep mutual learning. In *Proceedings of the IEEE Conference on Computer Vision and Pattern Recognition*, 4320–4328.

Zhou, H.; Yang, M.; Wang, J.; and Pan, W. 2019. BayesNAS: A Bayesian Approach for Neural Architecture Search. In *ICML*.

Supplementary Materials for Observations on K-image Expansion of Image-Mixing Augmentation for Classification

**Joonhyun Jeong^{*1}, Sungmin Cha^{*2}, Youngjoon Yoo^{1,3},
Sangdoo Yun³, Taesup Moon², and Jongwon Choi⁴**

¹ Face, NAVER Colva, ² Seoul National University, ³ NAVER AI Lab, ⁴ Chung-Ang University

{joonhyun.jeong, youngjoon.yoo, sangdoo.yun}@navercorp.com, {sungmin.cha, tsmoon}@snu.ac.kr, choijw@cau.ac.kr

Implementation Details of DCutMix

In this section, we present implementation details for DCutMix. Especially, we describe mixing process of DCutMix with pseudo-code in Algorithm 1. First, we sample variable ϕ from Dirichlet(α) as in Line 3. For $K-1$ iterations, we cut and mix $K-1$ image fractions on input. For each iteration, minibatch input and target are shuffled along the batch dimension. Then, an intermediate variable v is sampled from SBP using ϕ as in Line 7,8,13,14. The variable v determines width and height of the image patch to be mixed, where the exact position is bounded on the former image patch as in Line 16, 17. Then, we cut image patch from input_s and mix on input as in Line 18. In Line 19 ~ 27, the target soft label is also mixed by λ and λ_{last} , which denotes the exact area ratio of each mixed image patch.

Experiments and Analysis on DCutMix

This section contains detailed experiments and analysis of our proposed method DCutMix. We firstly conduct additional comparisons of our generalized K-image mixing augmentation methods with the augmentation methods mixing exactly two images in terms of loss surface. Second, we conduct ablation studies by modifying the hyperparameters of DCutMix. Third, we present implementation details of Saliency-DCutMix to resolve the label noise issue on ImageNet. Finally, we describe experimental settings to evaluate robustness against adversarial attacks and evaluation results of robustness against out-of-distribution data samples.

Plotting Three-Dimensional Loss Landscape

Here, we analyze the loss landscape patterns from various image mixing augmentation methods. To draw the patterns of loss landscape, we used PyHessian (Yao et al. 2019) and the detailed function of PyHessian is that, it provides an useful framework for estimating the trace of Hessian of the given neural network model. By using this function, we can draw the patterns of the loss landscape of the given neural network model by perturbing the given model’s parameters across the

first and second Hessian eigenvectors. The result in Figure 1 shows that our DCutMix and DMixup both have wider and lower loss landscape near local minima than CutMix and Mixup, respectively. When seeing the difference between Mixup and DMixup, we observed that our DMixup significantly stabilizes the loss landscape of Mixup which shows unstable loss landscape given perturbations on the model’s parameter.

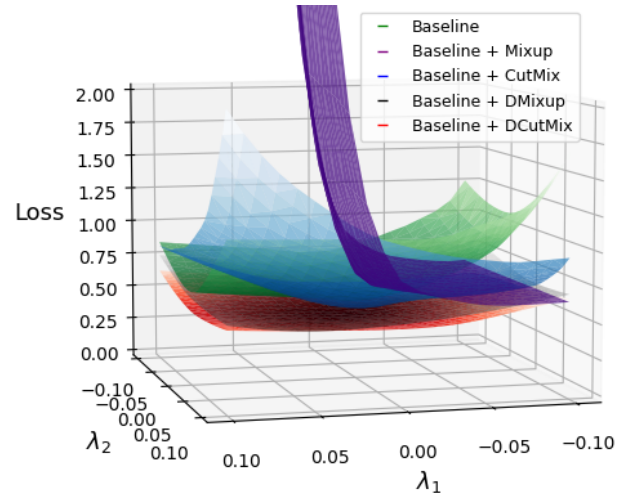


Figure 1: Comparison of image mixing augmentation in perspective of the loss landscape near local minima. λ_1 and λ_2 denote degree of perturbation on model parameters across top-1 and 2 eigenvectors of their Hessian matrix.

Effect of Mixing Multiple Images

We show the effect of mixing multiple images for augmentation on the classification task. The previous works, Zhang et al. (2017) and Kim et al. (2021), reported that mixing multiple images with the mixing ratios drawn from Dirichlet distribution degrades the classification performance. Unlike these results, we demonstrate that mixing multiple images with Dirichlet distribution as in Algorithm 1 enables a neural network model to obtain performance gain. For fair comparison, we used the equivalent training hyper-parameters, dataset (CIFAR-100) and backbone model (i.e. PreActResNet18),

^{*}These authors contributed equally.

Algorithm 1: Pseudo-code of DCutMix

Parameter: batch size N , number of mixing images K , parameter for Dirichlet distribution $\alpha \in \mathbb{R}^{N \times K}$.

```

1: for each iteration do
2:   input, target = get_minibatch(dataset)
3:   phi = batch_sample_dirichlet( $\alpha$ )
4:   for  $k \leftarrow 1$  to  $K - 1$  do
5:     input_s, target_s = shuffle_minibatch(input, target)
6:     if  $k == 1$  then
7:       v = phi[ $k$ ]
8:       mul_v = 1 - v
9:       prev_r_w, prev_r_h =  $W, H$ 
10:      prev_r_x, prev_r_y = 0, 0
11:      prev_target = target
12:    else if  $k \leq K - 1$  then
13:      v = phi[ $k$ ] / mul_v
14:      mul_v *= 1 - v
15:    end if
16:    r_w, r_h = Round(prev_r_w * Sqrt(1 - v)), Round(prev_r_h * Sqrt(1 - v))           // determine bbox to be cut.
17:    r_x, r_y = Unif(prev_r_x, prev_r_x + prev_r_w - r_w), Unif(prev_r_y, prev_r_y + prev_r_h - r_h)
18:    input[:, :, r_x:r_x+r_w, r_y:r_y+r_h] = input_s[:, :, r_x:r_x+r_w, r_y:r_y+r_h]
19:    lambda = (prev_r_w * prev_r_h - r_w * r_h) / (W * H)                                // adjust mixing ratio to be exact area ratio.
20:    if  $k == 1$  then
21:      target_mixed = lambda * prev_target
22:    else if  $k < K - 1$  then
23:      target_mixed += lambda * prev_target
24:    else
25:      lambda_last = (r_w * r_h) / (W * H)
26:      target_mixed += lambda * prev_target + lambda_last * target_s
27:    end if
28:    prev_r_w, prev_r_h = r_w, r_h
29:    prev_r_x, prev_r_y = r_x, r_y
30:    prev_target = target_s
31:  end for
32:  loss = compute_loss(model(input), target_mixed)
33:  model_update()
34: end for

```

as used in Kim et al. (2021)¹. Also, we selected the best sampling parameter for Dirichlet distribution $Dir(\alpha, \dots, \alpha)$ in $\alpha = \{\frac{1}{3}, \frac{1}{4}, \frac{1}{5}, \frac{1}{7}, 1\}$, as in Kim et al. (2021). Note that the result in Table ?? demonstrates the multiple image mixing augmentation method successfully obtains performance gain compared to two image mixing case, contrary to the result from Table 4 in Kim et al. (2021). Notably, our result shows consistent enhancement in top-1 error regardless of the number of mixing images compared to $K = 2$ case. We believe that this result again shows the advantage of expanding to multiple image mixing augmentation. These results also inform that DCutMix did not severely suffer from label noise issue caused by randomly cutting the image patch on CIFAR dataset, unlike on ImageNet (Yun et al. 2021).

¹We used the training settings from source code publicly available at <https://github.com/snu-mllab/Co-Mixup>.

K (# inputs for Mix) CutMix[‡] CutMix

| K | CutMix [‡] | CutMix |
|-----|---------------------|--------|
| K=2 | 21.29 | 21.34 |
| K=3 | 22.01 | 21.01 |
| K=4 | 22.20 | 20.5 |
| K=5 | - | 21.01 |
| K=7 | - | 20.9 |
| K=9 | - | 20.93 |

Table 1: (For Supplementary materials) Top-1 error rate tendency given mixing multiple images for CutMix on CIFAR-100 and PreActResNet18. [‡] denotes the reported result from Kim et al. (2021). We adopt the equivalent training hyper-parameters used in Kim et al. (2021) for fair comparison.

Sensitivity for Hyper-parameter

We tested the hyper-parameter sensitivity, $\alpha \in \mathcal{R}^K = \{\alpha, \dots, \alpha\}$, of our DCutMix and DMixup augmentations on classification performance. Table 2 empirically shows that

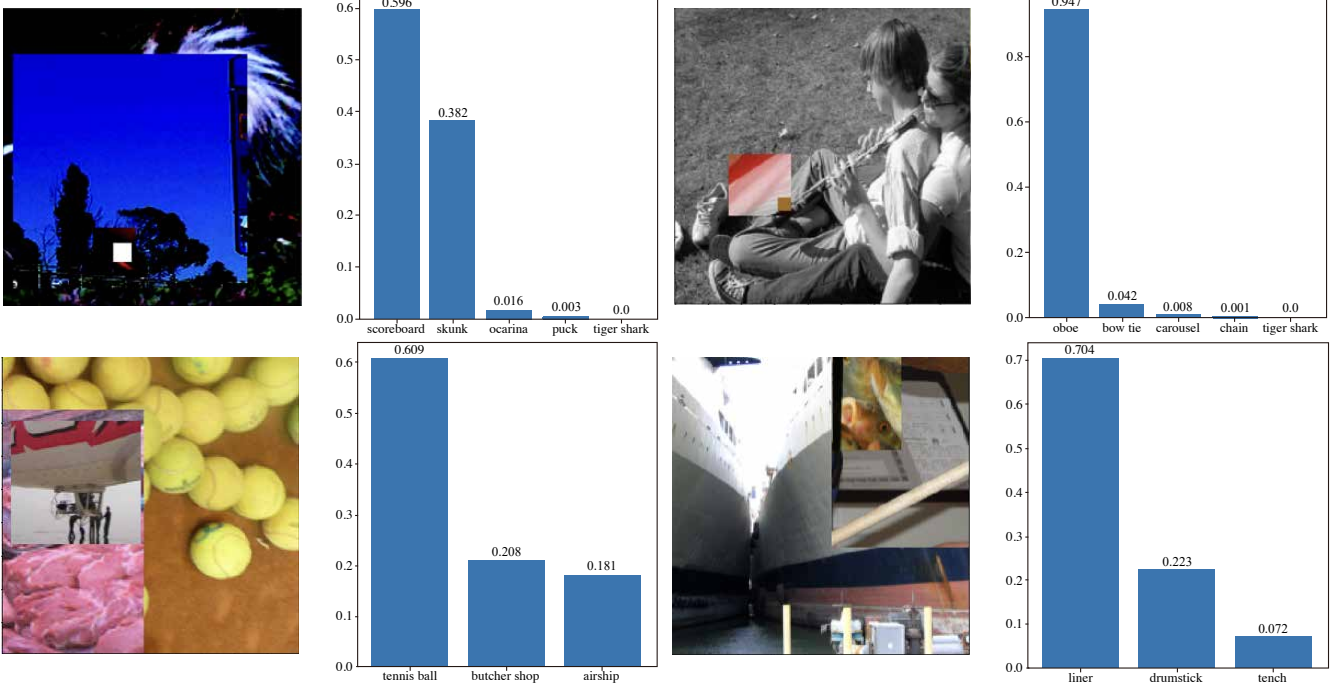


Figure 2: Qualitative example of augmented image and its soft label distribution for top K classes (top: DCutMix, bottom: Saliency-DCutMix). Note that for DCutMix case, visually salient information of top K classes are not fully contained (e.g. "Scoreboard" or "bow tie") in augmented image. Meanwhile, visually salient information of all the top K classes are fully contained for Saliency-DCutMix case.

DCutMix and DMixup work robustly to the variance of α .

| PyramidNet-200 | α | 0.1 | 0.3 | 0.5 | 0.7 | 1 | Std |
|----------------|----------|-------|-------|-------|-------|-------|------|
| + DMixup | | 15.68 | 15.35 | 15.58 | 15.80 | 15.07 | 0.28 |
| + DCutMix | | 14.74 | 14.18 | 13.67 | 14.23 | 13.86 | 0.40 |

Table 2: Top-1 error on CIFAR-100 depending on various α . Std denotes the standard deviation of the top-1 errors.

Saliency-DCutMix

In this section, we describe the implementation details of Saliency-DCutMix. Firstly, we obtain salient image patches by selecting the most salient pixel point of saliency-map as the center point, following Uddin et al. (2021). Here, width and height of each patch is given by eq (3) in the manuscript, for following Dirichlet distribution. Consequently, we mixed these salient image patches with SBP following DCutMix as in eq (4) in the manuscript.

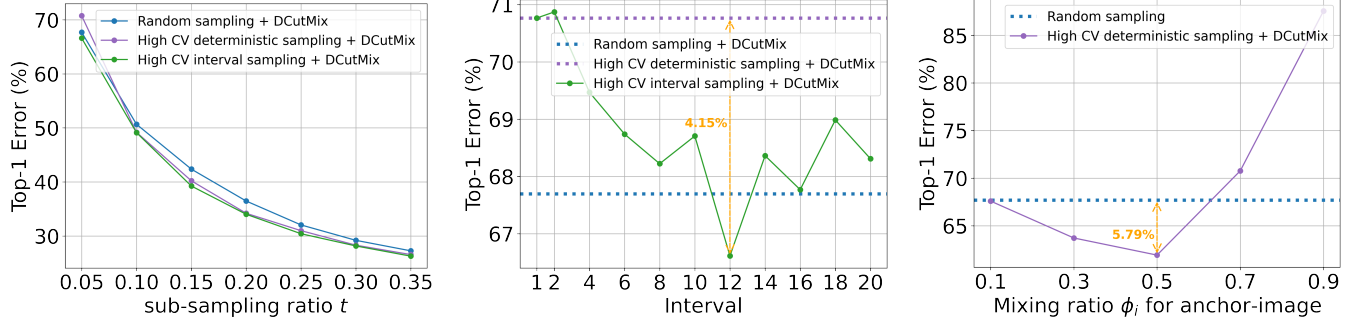
Figure 2 shows the qualitative examples of DCutMix and Saliency-DCutMix. Samples augmented with DCutMix contain background class objects other than ground truth object, which could lead to label noise when training. Meanwhile, samples augmented with Saliency-DCutMix show that the foreground class objects are mixed without background class objects being included.

Adversarial Robustness

In this section, we describe detailed experimental settings of adversarial robustness. Regarding white-box attack where attacker can freely access to the model's parameter, we use FGSM ℓ_∞ attack (Goodfellow, Shlens, and Szegedy 2014) with $\epsilon = 8$, following Yun et al. (2019). Black-box attack is more challenging situation, because attacker does not have any information about the target model to be attacked. For this case, we set a substitute model (*i.e.* ResNet152) and made adversarial examples by attacking it. Gray-box attack is a compromising setting between white- and black-box attack in that attacker knows the architecture of the model (*i.e.* ResNet50), while not accessing to the weight parameters of the model. Therefore, we generate adversarial examples using a substitute ResNet50 model trained with ImageNet dataset using a different random seed. For gray- and black-box attacks, we generated adversarial examples of ImageNet validation dataset using a more strong attack method called as PGD ℓ_∞ attack (Madry et al. 2017) with epsilon $\epsilon = 8$.

ImageNet-O

In order to evaluate robustness towards the out-of-distribution (OOD) data samples, we tested on ImageNet-O dataset (Hendrycks et al. 2021). ImageNet-O dataset contains OOD images whose class label do not belong to 1000 classes of ImageNet-1K dataset. The most ideal output of a classification model against the OOD data sample is to uniformly predict all classes with low confidence because a class in the



(a) Top-1 error plotting of ablations on selection function $S(\cdot)$.

(b) Top-1 error plotting with varying the sampling interval.

(c) Top-1 error plotting with varying anchor image mixing ratio ϕ_i

Figure 3: Ablation studies for data subsampling: Different selection function S (a), *interval-based* sampling depending on the various intervals (b), the impact of anchor image mixing ratio ϕ_i on the high CV *deterministic* sampling (c)

OOD dataset was not considered during training the classification model. These OOD images reliably cause various models to be misclassified with high confidence. To evaluate the robustness of each model against the OOD dataset samples, we measured area under the precision-recall curve (AUPR) on ImageNet-O dataset where higher AUPR denotes that the model robustly predicted OOD samples with lower confidence. In table 3, it is notable that the model trained without augmentation (Vanilla) showed best AUPR. All the augmentation methods are highly over-confident over the OOD samples, denoting fragility of the augmentation methods on label distribution shift.

| Model | ImageNet-O AUPR (%) |
|------------------|---------------------|
| Vanilla | 16.96 |
| Mixup | 16.30 |
| DMixup | 16.87 |
| CutMix | 15.85 |
| DCutMix | 16.73 |
| Saliency-DCutMix | 16.00 |

Table 3: Performance of various augmentation methods on ImageNet-O. We used ResNet-50 for all the methods. Vanilla denotes ResNet-50 trained without augmentation.

Data Subsampling

Implementation details

We describe the implementation details for the proposed subsampling framework. A newly subsampled set D for each class is defined as follows:

$$D = S(O(L_k) | k = j_1, \dots, j_{N_{intra}}, t), \quad (1)$$

where $O(\cdot)$ denotes the subsampling measure and $S(\cdot)$ denotes a sampling function indicating whether data sample x_k is to be included in D or not by using the subsampling ratio t . Here, j denotes the index of N_{intra} number of intra-class images where the class labels are equivalent among the others. $O(\cdot)$ is a proxy for subsampling; data samples are subsampled in order of O . With regard to the sampling

function $S(\cdot)$, it samples $t \times N_{intra}$ data samples based on the sampling measure $O(\cdot)$, which falls into two categories: a *deterministic* function sampling top $t \times N_{intra}$ samples sorted by $O(\cdot)$, and an *interval-based* function that collect samples sorted by $O(\cdot)$ with fixed interval.

Regarding the subsampling measure $O(\cdot)$, we employed the sample-wise uncertainty measure using Coefficient of Variation (CV), $\frac{\sigma(L_i)}{m(L_i)}$ (where L_i is derived from eq (8) in the manuscript). For estimating the sample-wise uncertainty, we set the number of non-anchor images $x \setminus x_i$ and their Dirichlet sampling parameter $\alpha \setminus \alpha_i$ as 2 and $\{\frac{2}{9}, \frac{2}{9}\}$, respectively. Additionally, we set the total number of sampling $\phi \setminus \phi_i$ from Dirichlet distribution, namely M , as 10.

Ablation studies

We conducted more detailed ablation studies for our high CV based subsampling method, in terms of the selection function $S(\cdot)$ and the anchor image mixing ratio ϕ_i , as shown in Figure 3. Regardless of the design choice of selection function $S(\cdot)$, all the high CV based subsampling methods outperformed the random sampling for $t \geq 0.1$, as shown in Figure 3a. Especially, selecting the high CV samples with interval showed the best classification performance among the various design choices of selection function. In Figure 3b, we showed the grid search result for finding the optimal interval value on subsampling ratio $t = 0.05$. The high CV sampling with optimally selected interval yields 4.15% lower error than the *deterministic* high CV sampling (i.e. interval=1), while showing 1.08% lower error compared to random subsampling case.

Figure 3c shows the impact of anchor image mixing ratio ϕ_i when the number of training samples is extremely small ($t = 0.05$). Note that the optimal $\phi_i = 0.5$ showed 5.79% better performance than the random sampling, when we set ϕ_i close to one, the performance significantly drops as the size of mixed region from non-anchor images becomes too small and non-discriminative to measure a robust uncertainty on the anchor image. Meanwhile, the case where ϕ_i value is close to zero (i.e. 0.1) does not contain enough fraction of anchor image, and hence the mixed images have little information of

the anchor image, leading the similar performance compared to the random sampling.

Comparison with other subsampling methods

We compare our proposed subsampling method with other subsampling methods employing various subsampling measures: *i*) *Uncertainty*: employing the predictive uncertainty measures (i.e. BALD, Variation Ratios (Gal, Islam, and Ghahramani 2017)) using Monte Carlo Dropout (Gal and Ghahramani 2016) and selecting highly uncertain data samples, *ii*) *K-Center Coreset* (Sener and Savarese 2017): greedily sampling center data such that the largest distance between a data point and its nearest center is minimized. Fig. 4 demonstrates that our subsampling method represents headroom compared to the other methods using uncertainty obtained from weight dropout (?) or sampling K-center core subset, especially when the size of the training data pool is extremely small.

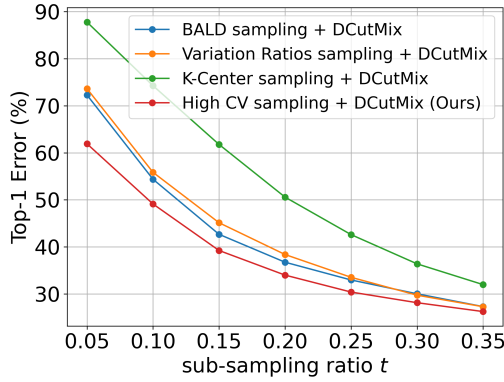


Figure 4: Comparison with various data subsampling methods.

Network Architecture Search

This section describes the detailed configurations of the experiments on network architecture search. For the searching process, we divided the subsampled (or entire) training dataset into two equal partitions, with one for optimizing the network parameters and the other one for optimizing the architecture hyper-parameters (i.e. α, β in Xu et al. (2019)). Also, we adopted the warm-up strategy in search process where only network parameters are optimized while α, β being freezed for the first 15 epochs as in Xu et al. (2019). Exceptionally, we applied the warm-up strategy for the first 5 epochs on the baseline method (i.e. searching on the entire dataset) where the number of total searching epochs is 10 (i.e. the left-most point for the Baseline in Figure 4b of manuscript). Additionally, we used Tesla V100 GPU for the searching process.

For the evaluation process where the searched network is trained from the scratch, we used the equivalent training hyper-parameters as in Xu et al. (2019).

References

Gal, Y.; and Ghahramani, Z. 2016. Dropout as a bayesian approximation: Representing model uncertainty in deep learning. In *international conference on machine learning*, 1050–1059. PMLR.

Gal, Y.; Islam, R.; and Ghahramani, Z. 2017. Deep bayesian active learning with image data. In *International Conference on Machine Learning*, 1183–1192. PMLR.

Goodfellow, I. J.; Shlens, J.; and Szegedy, C. 2014. Explaining and harnessing adversarial examples. *arXiv preprint arXiv:1412.6572*.

Hendrycks, D.; Zhao, K.; Basart, S.; Steinhardt, J.; and Song, D. 2021. Natural adversarial examples. In *Proceedings of the IEEE/CVF Conference on Computer Vision and Pattern Recognition*, 15262–15271.

Kim, J.; Choo, W.; Jeong, H.; and Song, H. O. 2021. Co-Mixup: Saliency Guided Joint Mixup with Supermodular Diversity. In *International Conference on Learning Representations*.

Madry, A.; Makelov, A.; Schmidt, L.; Tsipras, D.; and Vladu, A. 2017. Towards deep learning models resistant to adversarial attacks. *arXiv preprint arXiv:1706.06083*.

Sener, O.; and Savarese, S. 2017. Active learning for convolutional neural networks: A core-set approach. *arXiv preprint arXiv:1708.00489*.

Uddin, A. F. M. S.; Monira, M. S.; Shin, W.; Chung, T.; and Bae, S.-H. 2021. SaliencyMix: A Saliency Guided Data Augmentation Strategy for Better Regularization. In *International Conference on Learning Representations*.

Xu, Y.; Xie, L.; Zhang, X.; Chen, X.; Qi, G.-J.; Tian, Q.; and Xiong, H. 2019. Pcdarts: Partial channel connections for memory-efficient architecture search. In *International Conference on Learning Representations*.

Yao, Z.; Gholami, A.; Keutzer, K.; and Mahoney, M. 2019. PyHessian: Neural networks through the lens of the Hessian. *arXiv preprint arXiv:1912.07145*.

Yun, S.; Han, D.; Oh, S. J.; Chun, S.; Choe, J.; and Yoo, Y. 2019. Cutmix: Regularization strategy to train strong classifiers with localizable features. In *Proceedings of the IEEE International Conference on Computer Vision*, 6023–6032.

Yun, S.; Oh, S. J.; Heo, B.; Han, D.; Choe, J.; and Chun, S. 2021. Re-labeling imagenet: from single to multi-labels, from global to localized labels. In *Proceedings of the IEEE/CVF Conference on Computer Vision and Pattern Recognition*, 2340–2350.

Zhang, H.; Cisse, M.; Dauphin, Y. N.; and Lopez-Paz, D. 2017. mixup: Beyond empirical risk minimization. *arXiv preprint arXiv:1710.09412*.